1. Basic concepts

This chapter provides the basic concepts and models which are required for an understanding and interpretation of the investigated surface reactions. First, an overview over the basic ideas of surface reactions, their dynamics and the underlying theoretical concepts are presented. Since the investigated fs-laser induced surface reactions are substrate mediated, the laser excitation of the metal surface and its subsequent energy transfer mechanisms to the adsorbate are discussed.

1.1. Surface reactions

What happens when a molecule interacts with a surface? The purpose of this chapter is not to give an all-embracing answer to the posed question, but to point out essential characteristics concerning the special case of associative desorption of diatomic molecules, since this type of reactions has been investigated in the framework of the presented thesis. The potential energy surface (PES) governing such a chemical reaction is discussed and its influence concerning the reaction dynamics is explained. Since PESs are generally used within the adiabatic or Born-Oppenheimer approximation, a consideration of its validity and its breakdown is presented in a more formal way together with an illustration of the mechanisms, and the wide range of non-adiabatic effects in gas surface dynamics is given. Finally, the peculiarities of fs-laser induced surface reactions are summarized.

1.1.1. Associative desorption and dissociative adsorption

Associative desorption, also named recombinative desorption, denotes the formation of a molecule out of separately bound adsorbates during desorption. Its time-reversal, the dissociative adsorption, characterizes the breaking of a molecular bond during adsorption. In 1932, Lennard-Jones described the dissociation during adsorption of a diatomic molecule on a metal surface in terms of a combined one-dimensional potential energy surface [Len32]. Such a potential is shown in Fig. 1.1. The molecule-metal interaction is represented by the curve (X_2+metal)[1]. A molecule arriving at the surface along this curve finds an energetic minimum at z_p and binds either in a physisorbed state due to van-der-Waals interaction, or in a more strongly bound molecular chemisorbed state. Approaching closer to the surface leads to a strong repulsion due to the overlap between molecular and metal electron clouds. Curve (2X+metal) in the figure represents the interaction between two widely separated atoms and the metal where the cohesion energy of the atoms and surface exceeds the dissociation energy of the molecule, leading to a deeper energetic minimum at a closer distance z. In equilibrium,

[1] The presented considerations are valid without loss of generality for heteronuclear molecules, although X_2 denotes a homonuclear species.

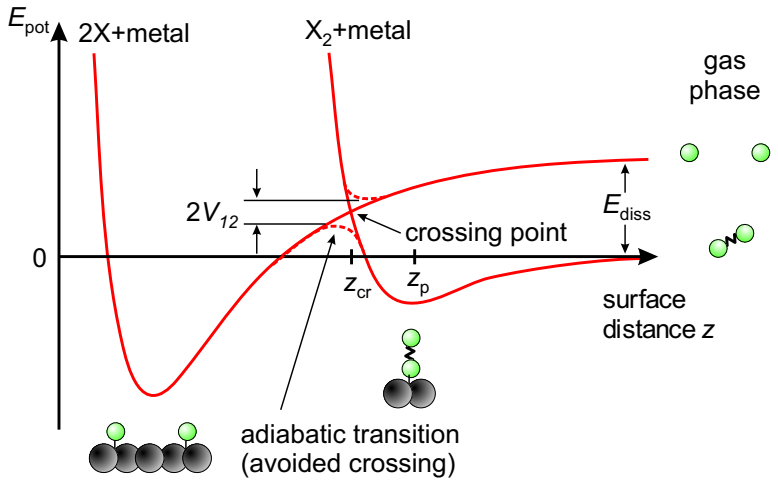

Figure 1.1.: Potential energy curve describing the interaction of a molecule with a metal surface. The molecular potential (X_2+metal) and the atomic PES (2X+metal) are depicted as a function of molecule-surface distance. In the adiabatic approximation the avoided crossing has a width that scales with the strength of the coupling V_{12} (see Section 1.1.3).

the adsorbed atoms are located at the minimum of curve (2X+metal). The difference between the two potential energy curves far from the surface is the molecular dissociation energy E_{diss}. A dissociation event occurs if a molecule approaches the surface until the crossing point of the two curves where it makes a transition from the molecular to the atomic PES leading to atomic adsorption. If this crossing point is positioned above zero in energy (with respect to the infinitely separated molecule-surface asymptote), the dissociation process is said to be activated[2]. A precursor state towards dissociation is formed at z_p. If, otherwise, the barrier is below zero, the molecule always exhibits enough energy for dissociation, which is then named non-activated.

An inconsistency in the presented description is that changing from the molecular to the atomic potential energy curve requires an instantaneously elongation of the molecular bond length. Lennard-Jones noted that although one-dimensional potential energy curves (as shown in Fig. 1.1) can prove great value in discussions, "they do not lend themselves to generalization when more than one coordinate is necessary to specify a configuration" [Len32]. Concerning diatomic molecules, it can be seen from Fig. 1.2(a), that a 6-dimensional (6D) PES is required for taking all molecular degrees of freedom into account. The center-of-mass position is given by x, y and z. The internal degrees of freedom of the molecule are described via θ, ϕ and d, where the first two define the orientation of the molecule and the last the intra-molecular bond length. Schematic two-dimensional (2D) cuts through a possible 6D PES are depicted in Fig. 1.2(b) and (c). These so-called elbow potentials include the two coordinates z and d "most important for a qualitative understanding of the dissociation process" [Dar95]. The entrance channel[3] in the upper left part of the PES represents the unperturbed molecule far away from the surface at large z, where typically a Morse-like potential along d accounts for the intra-molecular vibration. In the exit channel (lower right part of the PES), the molecular

[2]Note that the height of the dissociation barrier is generally much lower than E_{diss}. This causes the importance of heterogenous catalysis.

[3]The terminology originates historically from molecular beam experiments, where the PES is entered from the gas phase and left towards the adsorption state.

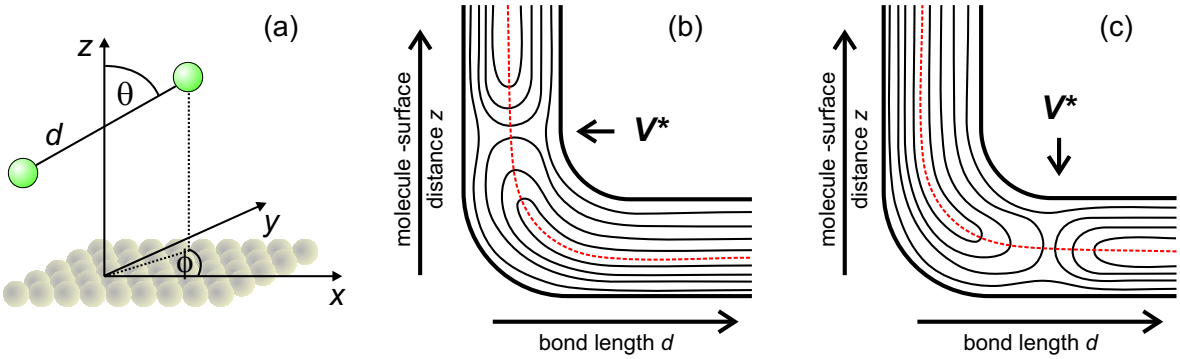

Figure 1.2.: (a) Coordinate system for the dissociation of a diatomic molecule on a surface. x, y and z are the center-of-mass coordinates, d the bond length and θ and ϕ the polar and the azimuthal angle respectively. (b)+(c) Schematic 2D cuts through a model 6D-PES are depicted. In such a so-called elbow plot, the potential energy is shown as function of z and d. The two scenarios for a so-called early (b) and a late barrier V^* (c) are depicted. The minimum energy reaction path is shown as a dashed line.

bond is broken and the potential along z describes the vibration of the two chemisorbed atoms at large d. These two extremes of the potential can be investigated either by gas phase or surface specific techniques. The more difficult part is the reaction zone, where the transition from the molecule to the adsorbed atoms (and vice versa) takes place.

1.1.2. Gas surface dynamics

The topology of the PES determines the dynamics of a chemical reaction [Eyr31, Pol72]. For activated processes, the location of the barrier plays a major role concerning the energy transfer between different molecular degrees of freedom [Hal90, Dar95]. Regarding an associative desorption process, the energy released into translation and vibration can be discussed by examining the 2D PES depicted in Fig. 1.2.

Figure 1.2(b) shows a PES with a so-called early barrier[4] located in the entrance channel. Crossing this barrier is required for desorption. The potential energy of the barrier V^* will be mainly released into the z coordinate which leads to an enhancement of translational over vibrational excitation in the desorbing molecules. In Fig. 1.2(c) a system characterized by a so-named late barrier is depicted. The barrier position is in the exit channel at an elongated molecular bond length. Crossing this barrier leads to vibrational excitation since the potential energy is released into the d coordinate. Vibrational energies larger than translational ones will be observed in the desorbing molecule flux. Summarizing, one can say that the position of the barrier determines the molecular coordinate and therefore the molecular degree of freedom into which the potential energy of the transition state is released. Therefore, early barriers are also attributed translational and late barriers vibrational, respectively. Concerning the dissociative adsorption, either vibrational pre-excitation or higher translational energies will lead to a higher sticking probability depending on the barrier location.

In non-activated reaction systems, an almost equally balanced energy partitioning among the different molecular degrees of freedom is found [Ren89, Wet01]. Smaller deviations from an energetic equipartition may result from dynamical steering, a process proposed by King

[4] ..., which is traversed pretty late regarding the desorption process

[Kin78]. This process can be understood taking into account the multi-dimensionality of the PES. Usually, the majority of reaction paths for different molecular orientations [Diñ00] and impact sites [Dar95, Wil96] exhibit energetic barriers hindering the process. Therefore, low kinetic or rotational energies help the particles to steer into an energetically favorable configuration leading to reaction. For example, this has been observed for the well studied system $H_2(D_2)$+Pd(100) [Ren89, Gro96b, Gro98, Eic99, Wet01]. Regarding the adsorption process this becomes evident from experiments performed by Rendulic et al. [Ren89], where a maximum in sticking (adsorption) probability is found for very low translational energies of the impinging molecules, corroborating the idea of steering and repelling as a function of interaction time. Desorption experiments performed by Wetzig et al. [Wet01] show an over-population of molecular states with low rotational quantum number. This so-called rotational cooling can be understood considering that for slowly rotating molecules the steering effect is strongly enhanced. It has to be mentioned that the experimental investigations alone do not give an unambiguous evidence for the dominance of the steering mechanism. Only in combination with 6D theoretical calculations [Eic99, Wet01], the concept of dynamical steering was corroborated and the experimental data very well reproduced. A detailed description can be found in a review article by Groß [Gro98].

As long as only molecular coordinates are considered for the dynamics taking place on the adiabtic PES (see Section 1.1.3), one should be aware that the above presented considerations do not take into account any energy transfer between substrate electrons or phonons and the adsorbate. This issue of adsorbate-substrate coupling is discussed in Section 1.3, whereas the origin of the coupling between electrons and adsorbate is explained in Section 1.1.3, and models for a qualitative understanding are presented in Section 1.1.4.

1.1.3. Theoretical concepts

The potential energy surfaces discussed in the previous sections are generally obtained by applying the adiabatic or Born-Oppenheimer approximation (BOA) since the dynamics of surface reactions are not exactly solvable due to the enormous number of degrees of freedom. The basic idea of the Born-Oppenheimer approximation [Bor27] is the assumption of a decoupling between nuclear and electronic motion. The huge difference in the velocities of electrons and nuclei due to their huge mass difference is used. The nuclei appear static for the electrons which in turn set up a PES governing the motion of the nuclei. This approach neglects excitation of the electronic system by nuclear motion since the electrons will always and instantaneously arrange to the lowest energetic configuration possible.

Generally and before applying any constraints, one can write the total Hamiltonian of N nuclei of mass M_N and n electrons as

$$\hat{H}_{\mathrm{tot}} = \hat{T}_{\mathrm{n}} + \hat{H}_{\mathrm{e}} = \hat{T}_{\mathrm{n}} + \hat{T}_{\mathrm{e}} + \hat{V}_{\mathrm{e-e}}(\boldsymbol{r}) + \hat{V}_{\mathrm{e-n}}(\boldsymbol{r},\boldsymbol{R}) + \hat{V}_{\mathrm{n-n}}(\boldsymbol{R}), \tag{1.1}$$

where $\boldsymbol{r}$, $\boldsymbol{R}$ represent the coordinates of the electrons and nuclei, respectively. $\hat{T}_{\mathrm{n}}$ and $\hat{T}_{\mathrm{e}}$ denote the operator of the kinetic energy of the nuclei and the electrons, respectively. The interaction potentials $\hat{V}_{\mathrm{e-e}}$, $\hat{V}_{\mathrm{e-n}}$ and $\hat{V}_{\mathrm{n-n}}$ describe the various Coulombic interactions between the charged particles. The wavefunction of the whole system $\psi(\boldsymbol{r},\boldsymbol{R},t)$ may be expanded using a suitable basis set of electronic wavefunctions $\{\phi_k(\boldsymbol{r},\boldsymbol{R})\}$ according to

$$\psi(\boldsymbol{r},\boldsymbol{R},t) = \sum_k \chi_k(\boldsymbol{R},t)\,\phi_k(\boldsymbol{r},\boldsymbol{R}). \tag{1.2}$$

The Schrödinger equation is then rearranged into a system of coupled equations of the form [Tul76]

$$\mathrm{i}\hbar\frac{\partial}{\partial t}\chi_k = \left(\hat{T}_\mathrm{n} + \hat{V}_{\mathrm{n-n}}\right)\chi_k + \sum_j \left(\left\langle \phi_k \middle| \hat{T}_\mathrm{e} + \hat{V}_{\mathrm{e-e}} + \hat{V}_{\mathrm{e-n}} \middle| \phi_j \right\rangle\right)\chi_j + \sum_j \hat{K}_{kj}\chi_j. \tag{1.3}$$

The coupling operators $\hat{K}_{kj}$ between nuclear and electronic motions

$$\hat{K}_{kj} = -\sum_N \frac{\hbar^2}{2M_N}\left(2\left\langle\phi_k\left|\nabla_{\boldsymbol{R}_N}\right|\phi_j\right\rangle\nabla_{\boldsymbol{R}_N} + \left\langle\phi_k\left|\nabla^2_{\boldsymbol{R}_N}\right|\phi_j\right\rangle\right), \tag{1.4}$$

depends on the velocities $\hbar\nabla_{\boldsymbol{R}_N}/M_N$ of the nuclei and the derivative of the electronic states with respect to nuclear position. Therefore, the energy transfer between electrons and nuclei is large if the velocities of the nuclei are large or if the electronic structure changes rapidly with $\boldsymbol{R}$.

Adiabatic or Born-Oppenheimer approximation

One chooses the ϕ_k to be eigenfunctions of the electronic part of the Hamiltonian $\hat{H}_\mathrm{e}$ with the nuclei treated fixed at position $\boldsymbol{R}$, which means that the $\phi_k = \phi_{k,\boldsymbol{R}}$ depend 'only' parametrically on $\boldsymbol{R}$ [Dar95]. Thus, the Schrödinger equation can be separated into a stationary electronic part

$$\hat{H}_\mathrm{e}\,\phi_{k,\boldsymbol{R}}(\boldsymbol{r}) = \left(\hat{T}_\mathrm{e} + \hat{V}_{\mathrm{e-e}} + \hat{V}_{\mathrm{e-n}} + \hat{V}_{\mathrm{n-n}}\right)\phi_{k,\boldsymbol{R}}(\boldsymbol{r}) = \epsilon_k(\boldsymbol{R})\,\phi_{k,\boldsymbol{R}}(\boldsymbol{r}), \tag{1.5}$$

and a time-dependent equation for the nuclei as

$$\mathrm{i}\hbar\frac{\partial}{\partial t}\chi_k(\boldsymbol{R},t) = \left[\hat{T}_\mathrm{n} + \epsilon_k(\boldsymbol{R})\right]\chi_k(\boldsymbol{R},t) + \sum_j \hat{K}_{kj}\chi_j(\boldsymbol{R},t). \tag{1.6}$$

The electronic energy ϵ_k fulfills the role of a potential function and constitutes the multi-dimensional PESs for the electronic state k like the ones discussed in Section 1.1.1 and in Section 1.1.2. The PESs (at least for the ground state) may be calculated from first principles using density functional theory (DFT) [Bri99, Gro98]. Transitions between electronic states are still induced by $\hat{K}_{kj}$, but if the electronic wavefunctions $\phi_{k,\boldsymbol{R}}$ vary only slowly with $\boldsymbol{R}$, their derivatives will be small, and if the nuclear velocities are also small, $\hat{K}_{kj}$ is negligible. This is the basis of the Born-Oppenheimer approximation, assuming that the nuclei appear always quasi-static with respect to the electron motion. The nuclear motion is then described by

$$\mathrm{i}\hbar\frac{\partial}{\partial t}\chi_k(\boldsymbol{R},t) = \left[\hat{T}_\mathrm{n} + \epsilon_k(\boldsymbol{R})\right]\chi_k(\boldsymbol{R},t). \tag{1.7}$$

In this approximation, the electronic state k of the system is fixed at all times, which is the reason that the Born-Oppenheimer approximation is also termed the adiabatic approximation. Moreover, the total energy of the nuclei is conserved.

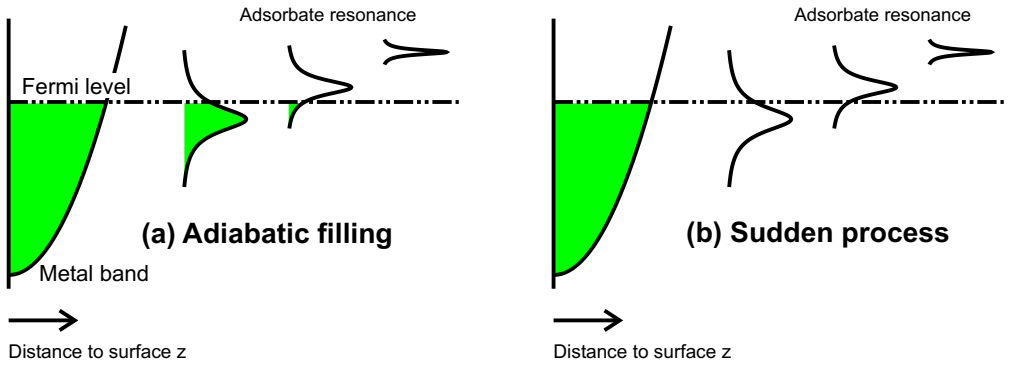

Figure 1.3.: As a molecule approaches a metal surface, the sharp molecular electronic states shift and broaden to such an extent that they can cross the Fermi level ϵ_F. Shown is the schematic representation of the dynamical interaction corresponding to the adiabatic and sudden limits. If the molecule moves slowly, the affinity levels fills adiabatically, and the motion is determined by the PES of the electronic ground state. If the molecule moves quickly, the empty states below ϵ_F represent an electronic excitation of the system and a breakdown of the BOA. Scheme adapted from [Hol91].

Breakdown of the Born-Oppenheimer approximation

As can be shown by first order perturbation theory [Gri81b], Eq. (1.7) is only valid if $\hat{K}_{kj} \ll |\,\epsilon_k(\boldsymbol{R}) - \epsilon_j(\boldsymbol{R})|$, i.e. if the coupling is significantly less than the level spacing. This is definitely not the case for metal surfaces, where the level spacing at the Fermi level ϵ_F is arbitrarily small. When a molecule approaches a metal surface, its affinity level drops and broadens to such an extent that it can cross ϵ_F [Hol91] as depicted in Fig. 1.3. At low incoming velocities, it is successively occupied by electrons from the substrate, i.e. it fills adiabatically. At high velocities, the state remains empty below ϵ_F, the system is left electronically excited. Such a sudden process is depicted on the right of Fig. 1.3. This dynamical interaction corresponds to the velocity dependent term of the coupling operator $\hat{K}_{kj}$. De-excitation of the excited system may occur by radiative transitions, Auger decay or electron-hole pair generation. The latter will dissipate translational energy from the impinging molecule to the electronic system of the substrate, which can be described in terms of a macroscopic quantity, the electronic frictions (see Section 1.3 and Section 1.1.4).

Beside the dependence on the velocities of the nuclei, the non-adiabatic coupling term becomes large, if the change in electronic structure with respect to nuclear positions is large. As can be seen from Fig. 1.1, this is the case at the transition state, where small changes in the nuclei positions lead to large changes of the electronic structure since strong mixing between the molecular orbitals and the substrate bands occurs [Lun05, Lun06].

Diabatic representation

Instead of describing electronic excitations in terms of coupling between adiabatic states $\phi_{k,\boldsymbol{R}}$, one can use a diabatic electronic basis $\{\xi_k(\boldsymbol{r})\}$ [Tul76], which is independent of the nuclear coordinates $\boldsymbol{R}$:

$$\psi(\boldsymbol{r}, \boldsymbol{R}, t) = \sum_k \zeta_k(\boldsymbol{R}, t)\, \xi_k(\boldsymbol{r})\,. \tag{1.8}$$

The diabatic states ξ_k are introduced to describe the system in possible excited states. As can be seen from Eq. (1.4), $\hat{K}_{kj} = 0$ in this representation, and the Schrödinger equation has

again the form of Eq. (1.6), but now as a matrix equation

$$\mathrm{i}\hbar\frac{\partial}{\partial t}\zeta_k\left(\boldsymbol{R},t\right)=\left[\hat{T}_{\mathrm{n}}+V_{kk}\left(\boldsymbol{R}\right)\right]\zeta_k\left(\boldsymbol{R},t\right)+\sum_{k\neq j}V_{kj}\zeta_j\left(\boldsymbol{R},t\right), \tag{1.9}$$

where the diagonal elements V_{kk} of the potential represent a set of potential energy surfaces coupled by the off-diagonal elements

$$V_{kj}\left(\boldsymbol{R}\right)=\left\langle\xi_k\left|\,\hat{T}_{\mathrm{e-e}}+\hat{V}_{\mathrm{e-e}}\left(\boldsymbol{r}\right)+\hat{V}_{\mathrm{e-n}}\left(\boldsymbol{r},\boldsymbol{R}\right)\right|\zeta_j\right\rangle. \tag{1.10}$$

The Lennard-Jones model, described in Section 1.1.1 and depicted in Fig. 1.1, is such a diabatic representation consisting of an electronic state for the intact molecule X_2, which exhibits the lower energy far from the surface, whereas the electronic state for two separated atoms X constitutes the ground-state for atomic chemisorption on the surface. The potential in this representation is a 2×2 matrix

$$V=\begin{pmatrix}V_1 & V_{12}\\ V_{12} & V_2\end{pmatrix}, \tag{1.11}$$

where the coupling V_{12} is a measure of the extent to which mole that diabatic states but rather in a superposition of both with a weighting determined by V_{12}. An adiabatic description can be obtained by diagonalizing V to get [Dar95]

$$V_{\pm}=\frac{1}{2}\left[\left(V_1+V_2\right)\pm\sqrt{\left(V_1-V_2\right)^2+4V_{12}^2}\right]. \tag{1.12}$$

From this it can be seen that the adiabatic PESs, V_+ and V_- are separated by $2V_{12}$ at the crossing point $V_1=V_2$. This so-called avoided crossing is depicted in Fig. 1.1. The BOA is more likely to be valid if V_{12} is large, but usually its value is not known [Dar95].

As will be shown in the following sections, the coupling between substrate electrons and adsorbate nuclei also offers the possibility for a fs-laser induced non-adiabatic desorption mechanism. This mechanism can be either described by a phenomenological model in the diabatic framework leading to desorption induced by multiple electronic excitations (DIMET) [Mis92], or in terms of an electronic frictional coupling between thermalized electrons and the adsorbate [New91, Bra95], whereby the adsorbate remains on the adiabatic ground state PES. The latter so-called 'nearly' adiabatic representation as well as the DIMET approach will both be introduced in the next section, where their usefulness regarding different physical systems is discussed.

1.1.4. Non-adiabatic effects in surface reactions

Electronic excitations during adsorption

During exothermic adsorption on a metal surface, the released energy is transferred from the reaction complex into the nuclear and electronic degrees of freedom of the metal substrate. Possible subsequent elementary processes are illustrated in Fig. 1.4. The direct energy transfer to phonons is adiabatic. Concerning molecular adsorption, the strength of adiabatic coupling depends strongly on the involved molecular coordinates. The translational coordinate z couples strongly to the lattice via momentum transfer [Ger87], whereas the vibrational

coordinate d couples only weakly to phonons and strongly to electrons. The latter becomes obvious regarding vibrational lifetimes of molecules either adsorbed on a metal or on an insulator surface. The lifetime for vibrational relaxation of CO adsorbed on an insulating NaCl surface has been measured to be about $\sim 10^{-4}$ s [Cha90], whereas the lifetime on Cu(100) is about 2 ps [Mor92].

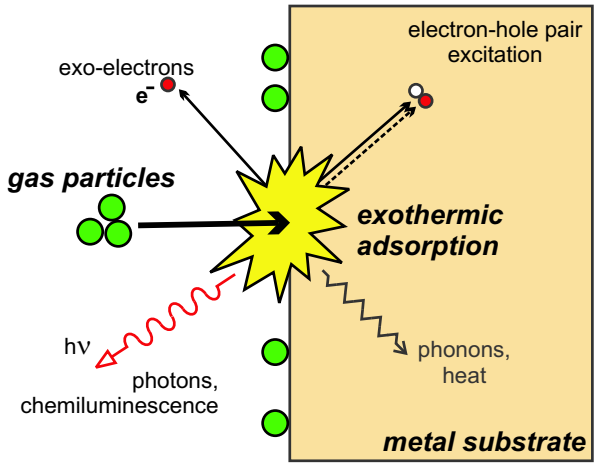

Figure 1.4.: Schematic depiction of an exothermic adsorption on a metal substrate. The induced elementary excitations of the substrate can lead to photon and exoelectron emission or to e-h pair or phonon generation. The scheme is adapted from [Nie02].

Direct evidence that non-adiabatic excitation takes place upon adsorption is obtained from the observation of emitted electrons or photons during the reaction. Excited electrons with sufficient energy larger than the work function may overcome the surface barrier leading to emission of chemically induced exoelectrons into vacuum. Generated photons may also leave the metal and this effect is called surface chemiluminescence. Both phenomena have been observed in a special class of highly exothermic surface reaction of reactive molecules with mainly electropositive metals (e.g. halogens/alkali metals). An overview of these effects is given by the reviews of Greber [Gre97] and Nienhaus [Nie02].

Less exothermic adsorption, which does not lead to exoelectron or photon emission, may generate electronic excitations in the metal substrate. The direct experimental confirmation of this process has to be much more sophisticated, since the electrons equilibrate within a ps time scale with the lattice (see Section 1.2.1). A new experimental approach was introduced that allows detection of chemically created electron and hole pairs [Ger01, Nie02]. A metal-insulator (Schottky) contact is used, where the excited electrons travel ballistically through the thin metal film. Reaching the semiconductor, the electrons are detected as so-named chemicurrents. An excitation probability of 6 to 100 % is reported, corroborating the importance of electronic energy dissipation during adsorption on metal surfaces [Ger01, Nie02].

Desorption induced by electronic excitations

Since desorption is the time-reversal of adsorption, it is obvious that coupling between excited substrate electrons and the nuclei of an adsorbate may also lead to desorption. Before discussing non-adiabatic desorption mechanisms, a brief description of the adiabatic, phonon

mediated one is presented: On the left of Fig. 1.5 a so-called ladder climbing process is depicted. The substrate atoms couple their vibrations to the adsorbate until enough kinetic energy is collected to overcome the barrier towards desorption. The dynamics of this process are completely determined by the electronic ground state potential energy curve, and the adsorbate is in thermal equilibrium with the substrate.

Non-adiabatic excitation mechanisms are depicted in Fig. 1.5(b) and (c). Using the diabatic representation, the chemistry can be rationalized by desorption induced by electronic transitions (DIET) (Fig. 1.5(b)) involving HOMO (highest occupied molecular orbital) and LUMO (lowest unoccupied molecular orbital) states. In this scenario, hot electrons scatter from the HOMO into a higher lying resonance state, the LUMO, and induce forces on the nuclei in the excited state since the equilibrium distances are different for both states. After some femtoseconds, de-excitation takes place, and the adsorbate returns with some gained vibrational excitation to the ground state potential and desorbs. The theoretical framework for this process was developed by Menzel, Gomer and Redhead [Men64, Red64], and the MGR model for the case of a repulsive excited potential was established. Antoniewicz showed that the same formalism can also be applied for binding excited states with an equilibrium position closer to the surface [Ant80]. If a single excitation is not sufficient to couple enough energy to the nuclear degrees of freedom of the adsorbate to overcome the reaction barrier, multiple excitations can do. This DIMET (desorption induced by multiple electronic transitions) process was suggested by Misewich et al. [Mis92] to explain electron mediated desorption from surfaces after fs-laser excitation. With the high hot electron densities induced by an ultrashort light pulse, vibrational excitation rates can exceed the rates of vibrational damping, and the resulting vibrational up pumping in the ground electronic state then leads to desorption. A disadvantage of this model is the lack of knowledge about the involved excited PES and its lifetime, so that mainly a qualitative understanding of the experiments can be obtained [Mis92].

Another theoretical approach rationalizes the electron mediated chemistry in terms of an

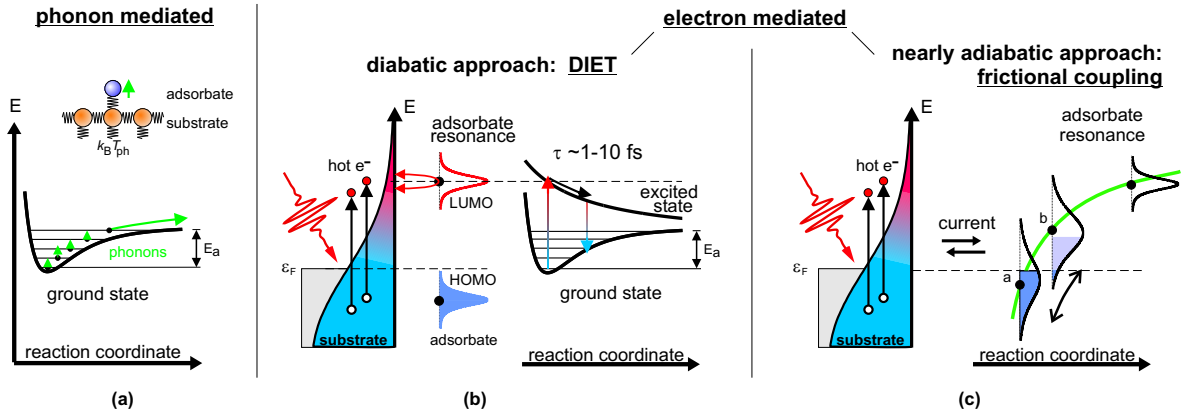

Figure 1.5.: Schematic 1D illustration of the possible energy transfer mechanisms leading to desorption. (a) Adiabatic phonon mediated process: Due to coupling between vibrating substrate atoms and the adsorbate, the energy required for desorption is transferred into the adsorbate via so-called vibrational ladder-climbing. The dynamics are determined by the ground state potential. (b)+(c) Non-adiabatic mediated desorption mechanisms: Excitation via an electronic transition to a higher lying repulsive state (b) and via frictional coupling between adsorbate and hot electrons (c) are illustrated. Their applicability with respect to different physical regimes is discussed in the text.

electronic frictional coupling between the adsorbate and the thermalized hot electrons [New91, Bra95], depicted in Fig. 1.5(c). This mechanism can be understood as the time-reversed process of vibrational damping on metal surfaces: the adsorbate vibration leads to a motion along the reaction coordinate and therefore to an energetic shift of its resonance with respect to the Fermi level ϵ_F. Unoccupied states below ϵ_F will force substrate electrons to scatter into the resonance, whereas electrons in states higher than ϵ_F will scatter back into the substrate. This adsorbate motion induced electron-hole (e-h) pair creation is summarized to the macroscopic quantity of frictional coupling. On the other hand, this coupling allows hot electrons to exert fluctuating forces on the nuclear coordinates and induce chemistry. Since excitation of highly delocalized electrons only marginally alters the local shape of the potential energy surface [Hea95], the motion of the adsorbate is considered to take place on a single "effective" PES out of a continuum of nearly parallel energy surfaces. Usually the adiabatic ground state potential serves as effective potential and the representation is named nearly adiabatic.

Depending on the system, either the DIET/DIMET or the frictional approach may be more suited. For high-lying quasilocalized adsorbate states and negative ion-type resonances, a diabatic representation seems to be more appropriate, since the electronic structure changes considerably and the assumption of an unchanged effective electronic ground state fails. This indicates the range of use for the frictional description, namely systems not having any long-lived (narrow) adsorbate induced resonance states. It has been suggested that intermediate regimes can be described in part via an electron temperature dependent electronic friction, which is small at low temperatures and increases strongly if the temperature is large enough to populate significantly the adsorbate resonance [Bra95]. The adsorbate-substrate coupling discussed in Section 1.3 is modeled within the frictional framework, which is believed to describe femtochemistry on metal surfaces much better [Lun06].

Independent of the chosen representation, one has to keep in mind that the reaction dynamics are no longer exclusively determined by the ground state PES, since either the gradient of a multidimensional excited PES or a multi-dimensional friction coefficient, respectively, contribute to the process of interest.

1.1.5. Femtosecond laser induced surface reactions

Having described the more general aspects of surface reactions in the previous sections, the purpose of this section is to highlight the peculiarities of fs-laser induced surface reactions. A schematic diagram illustrating the energy flow after fs-laser excitation is depicted in Fig. 1.6. Due to the marginal thickness of few adsorbate layers, direct optical excitation of the adsorbate can be neglected for the systems investigated in the framework of this thesis. The excitation of the metal surface after fs-laser irradiation is typically described in terms of the two temperature model (2TM), where the electron and lattice responses to the fs-laser pulse are represented by two coupled heat baths (Section 1.2).

As shown in the previous sections, coupling to the adsorbate may either occur by phonons or by electrons. This is depicted in Fig. 1.6, where typical coupling times are given for the two channels [Fri06]. For times of few picoseconds following fs-laser excitation, a regime with $T_{el} \gg T_{ph}$ is accessible (Section 1.2), which in combination with a two-pulse correlation experiment (Section 1.3.4) allows to distinguish between electron and phonon mediated reaction channels.

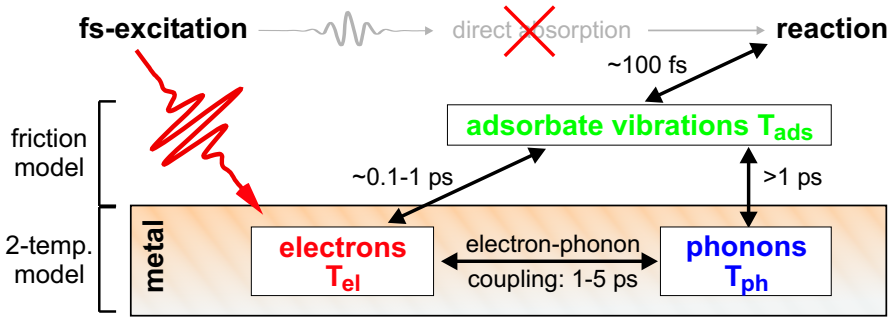

Figure 1.6.: Schematic diagram of the energy flow after fs-laser excitation of an adsorbate covered metal surface. Typical timescales for the various couplings are denoted. Since direct optical excitation by the adsorbate can be neglected, a substrate mediated process has to be taken into account.

This means that the *identification and investigation of non-adiabatic surface reactions is feasible with fs-laser excitation.* The models describing the adsorbate substrate coupling are introduced in Section 1.3.

1.2. fs-laser excitation of metal surfaces: the two temperature model

The excitation of the metal surface due to fs-laser irradiation is discussed. Therefore, the macroscopic quantities reflection and absorption have to be correlated to a microscopic description in terms of the interaction between the light field (respectively the photons) and the metal electrons. The absorption is due to the creation of electron-hole (e-h) pairs which thermalize via electron-electron scattering and cool down to thermal equilibrium with the phonon temperature because of electron-phonon scattering and diffusion. The temporal evolution of the transient electron and phonon temperatures T_{el} and T_{ph} can be described via the two-temperature model, which is based on the following assumptions:

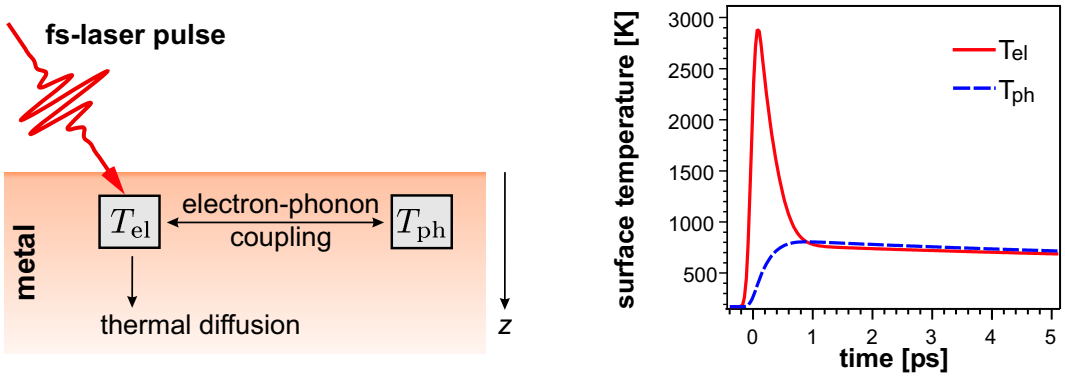

Figure 1.7.: Two-temperature model scheme (left) [Ani74] and an example for the transient electron and phonon surface temperatures T_{el} and T_{ph} after fs-laser excitation of ruthenium with a 100 fs, 800 nm laser pulse and a fluence of $\langle F \rangle = 60\,\mathrm{J/m^2}$. Electronic peak temperatures of several thousand Kelvin are achievable.

The absorption of light induces an instantaneously thermalized hot-electron distribution, represented by an electron heat bath, whose energy content is expressed by a Fermi-Dirac distribution with T_{el}. This electron heat bath transfers energy either to the substrate by thermal diffusion or to a phonon heat bath via electron-phonon coupling. The phonon heat bath is characterized by T_{ph} of a Bose-Einstein distribution which represents the energy content in this subsystem. The scheme of the two coupled heat baths is depicted in Fig. 1.7. The temporal evolution of the energy contents in the electronic and phononic sub-systems are represented by a set of coupled differential equations [Ani74]:

$$\begin{aligned} & & \text{thermal diffusion} & & \text{e-ph coupling} & \quad \text{excitation} & \\ C_{\mathrm{el}}(T_{\mathrm{el}})\frac{\partial}{\partial t}T_{\mathrm{el}} &= \frac{\partial}{\partial z}\left(\kappa_{\mathrm{el}}\frac{\partial}{\partial z}T_{\mathrm{el}}\right) & - H(T_{\mathrm{el}},T_{\mathrm{ph}}) + & \quad S(z,t) & \text{(1.13a)} \\ C_{\mathrm{ph}}(T_{\mathrm{ph}})\frac{\partial}{\partial t}T_{\mathrm{ph}} &= & + H(T_{\mathrm{el}},T_{\mathrm{ph}}) & & \text{(1.13b)} \end{aligned}$$

The first equation describes the temporal change in the energy content of the electron gas which is due to absorption of the laser pulse $S(z,t)$, energy transfer to the lattice $H(T_{\mathrm{el}},T_{\mathrm{ph}})$ via electron-phonon coupling and due to transport into the bulk via diffusion. z denotes the distance from the surface into the bulk. It is sufficient to apply the calculations only to this

electronic heat capacity	γ_{el}	400	$\mathrm{Jm^{-3}K^{-2}}$	[Kit96]
electronic heat conductivity	κ_0	117	$\mathrm{Wm^{-1}K^{-1}}$	[Kit96]
Debye temperature	θ_{D}	404	K	[Sch81]
electron-phonon coupling constant	g_∞	185	$10^{16}\,\mathrm{Wm^{-3}K^{-1}}$	[Bon00a]
refractive index (400 nm)	$n_{\mathrm{r}} + \mathrm{i}\, n_{\mathrm{i}}$	$2.40 + \mathrm{i}\, 4.64$		[Wea81]
refractive index (800 nm)	$n_{\mathrm{r}} + \mathrm{i}\, n_{\mathrm{i}}$	$5.04 + \mathrm{i}\, 3.94$		[Wea81]
optical penetration depth (400 nm)	δ	6.9	nm	
optical penetration depth (800 nm)	δ	16.2	nm	

Table 1.1.: Physical properties of ruthenium. The optical penetration depth is calculated with Eq. (1.18).

coordinate since the size of the laser spot is large compared to the optical penetration depth and the lateral thermal diffusion lengths.

The specific heat capacity of the electrons C_{el} depends on T_{el} and is given by [Ash01]

$$C_{\mathrm{el}} = \gamma_{\mathrm{el}} T_{\mathrm{el}}, \tag{1.14}$$

whereby a constant density of states at the Fermi Level is assumed. γ_{el} is the coefficient of the electronic heat capacity. Due to this small electronic heat capacity γ_{el}, transient electron temperatures of several thousand Kelvin are achievable, as can be seen in a model calculation depicted on the right of Fig. 1.7.

The temperature dependence of the electron thermal conductivity[5] can be approximated via [Kan98]

$$\kappa_{\mathrm{el}} \approx \kappa_0 \frac{T_{\mathrm{el}}}{T_{\mathrm{ph}}}, \tag{1.15}$$

with κ_0 being an empirical electron heat conductivity. Values for γ_{el} and κ_0 are given in Table 1.1.

Equation (1.13b) denotes the transient energy in the lattice which is described by T_{ph} and the heat capacity C_{ph}, which is according to the Debye model [Ash01]

$$C_{\mathrm{ph}}(T_{\mathrm{ph}}) = 9 N_{\mathrm{A}} k_{\mathrm{B}} \left(\frac{T_{\mathrm{ph}}}{\theta_{\mathrm{D}}} \right)^3 \int_0^{\theta_{\mathrm{D}}/T_{\mathrm{ph}}} \mathrm{d}x \frac{x^4 \mathrm{e}^x}{\left(\mathrm{e}^x - 1\right)^2}. \tag{1.16}$$

For $T_{\mathrm{ph}} > \theta_{\mathrm{D}}$, Eq. (1.16) passes into the Dulong-Petit law where a constant heat capacity of $C_{\mathrm{ph}} = 3 N_{\mathrm{A}} k_{\mathrm{B}} \approx 25\,\mathrm{Jmol^{-1}} K^{-1}$ is derived. The Debye temperature θ_{D} for ruthenium is also given in Table 1.1.

The optical excitation $S(z,t)$ and the electron-phonon coupling $H(T_{\mathrm{el}}, T_{\mathrm{ph}})$ will be discussed in the following sections which then allows to calculate the transient electron and phonon temperatures after fs-laser excitation.

Equations (1.13) have to be solved numerically, and details concerning the numerical implementation can be found in [Fun99, Den99].

[5] In metals, the phononic contribution κ_{ph} to the heat transport can be neglected since $\kappa_{\mathrm{ph}}/\kappa_{\mathrm{el}} \leq 1 \cdot 10^{-5}$ [Ash01].

1.2.1. Optical excitation and thermalization of the electrons

Irradiation of a metal surface with light leads either to reflection due to coherent radiation of the induced polarization or to absorption by the creation of electron-hole pairs. The absorption along the direction of propagation z perpendicular to the surface is given by the Lambert-Beer law

$$I \propto \mathrm{e}^{-z/\delta}, \tag{1.17}$$

where the optical penetration depth δ is correlated via

$$\delta = \frac{\lambda}{4\pi n_\mathrm{i}} \tag{1.18}$$

to the wavelength λ and the imaginary part of the refractive index n_i. The reflectivity of the metal surface is described by the Fresnel formulas, whereby one has to distinguish the reflection coefficients for the parallel and perpendicular polarization $R_\parallel$ and $R_\perp$ respectively. Both are given as function of the angle of incidence α and the complex refractive index $n = n_\mathrm{r} + \mathrm{i}\, n_\mathrm{i}$ of the irradiated material [Fli97]:

$$R_\parallel = \left| \frac{2n \cos\alpha}{n^2 \cos\alpha + \sqrt{n^2 - \sin^2\alpha}} \right|^2, \tag{1.19a}$$

$$R_\perp = \left| \frac{\cos\alpha - \sqrt{n^2 - \sin^2\alpha}}{\cos\alpha + \sqrt{n^2 - \sin^2\alpha}} \right|^2. \tag{1.19b}$$

The reflection coefficients $R_\parallel$ and $R_\perp$ as a function of the angle of incidence α are depicted in Fig. 1.8 for the typical wavelengths of 800 and 400 nm, which are also used in the experiments described in Chapter 2. The refractive indices are denoted in Table 1.1.

The overall optical excitation as a function of z and t is then given by

$$S(z,t) = \frac{(1-R)\cdot I(t)}{\delta} \cdot \mathrm{e}^{-z/\delta}. \tag{1.20}$$

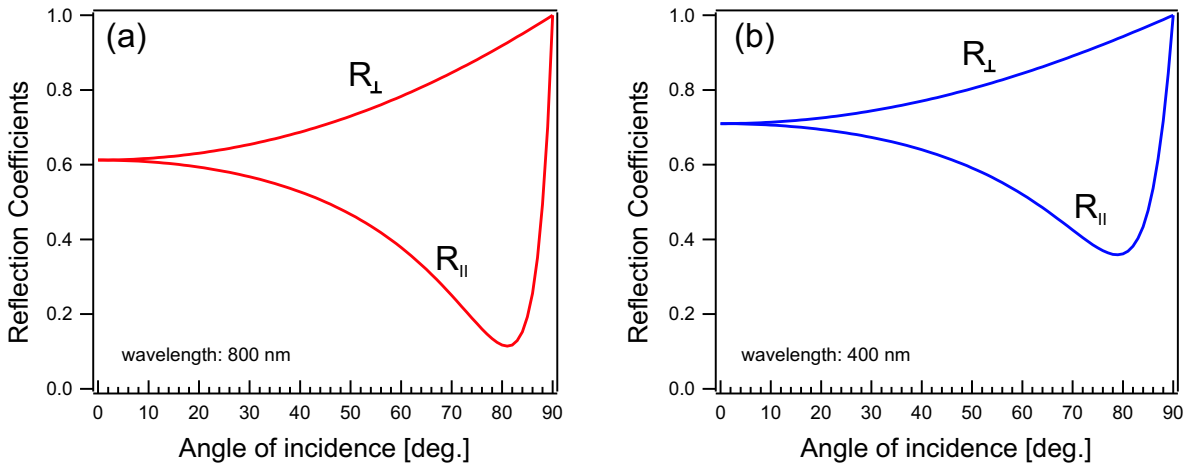

Figure 1.8.: Reflection coefficients $R_\parallel$ and $R_\perp$ for ruthenium as a function of the angle of incidence according to Eq. (1.19). The coefficients are plotted for the two wavelengths of 800 nm (left) and 400 nm (right).

The laser intensity $I(t)$ is assumed to be Gaussian in time. Applying Eq. (1.20) to the 2TM model implies that the electrons thermalize directly after optical excitation, and that the energy content in the electronic subsystem can be described by a temperature $T_{\mathrm{el}}(z,t)$ and the Fermi-Dirac statistics.

Thermalization of the electron gas

The processes following directly after the optical excitation of a metal surface are depicted in Fig. 1.9. Before optical excitation, the electrons can be described according to a Fermi-Dirac distribution with temperature T_0. The optical excitation with a laser pulse of photon energy $h\nu$ moves an almost rectangular distribution of electrons above the Fermi level E_{F}. The resulting distribution is not thermalized, i.e. it can not be described with a distribution function of a distinct temperature T_{el}. Due to electron-electron scattering, the electrons thermalize and can again be characterized by $T_{\mathrm{el}} > T_0$.

Since a thermalized electron distribution is required for the applicability of the 2TM, it is important to verify the assumption of an instantaneous thermalization. Thermalization times of several 10 fs up to a few ps are reported [Wol98]. These times depend on the excitation parameters as well as on the metal. The thermalization time decreases with increasing excitation densities [Fan92b, Fan92a, Ret02, Lis04]. The reason for this behavior is the increasing number of occupied and unoccupied electronic states around the Fermi level, i.e. a larger phase space for scattering events is available for thermalization. In addition, a strong non-thermal electron distribution is soonest comparable with a Fermi-Dirac distribution [Ret02].

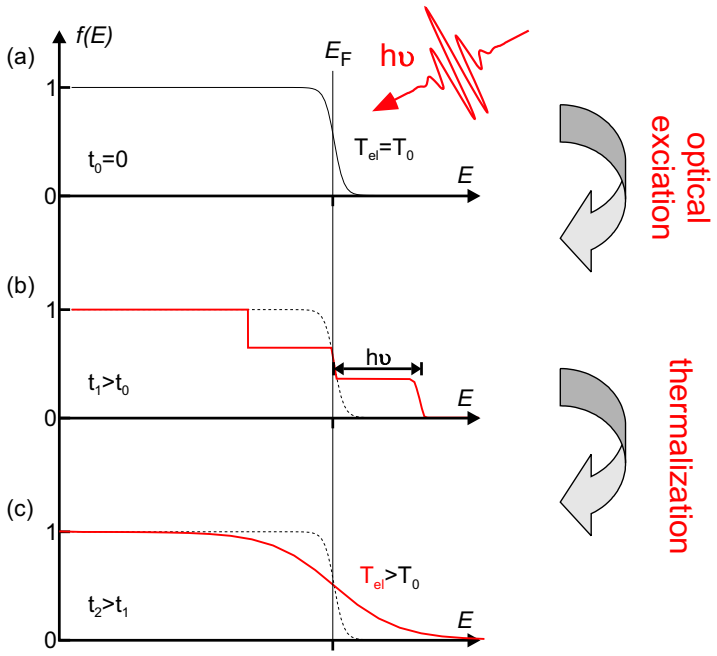

Figure 1.9.: Schematic diagram for the thermalization of an optically excited electron gas: (a) Before excitation, the Fermi-Dirac distribution is characterized by a temperature T_0. (b) Due to optical excitation, an almost rectangular distribution is moved above the Fermi level which leads to a highly non-thermal distribution. (c) Due to electron-electron scattering an energy redistribution takes place, i.e. the electrons thermalize and a Fermi-Dirac distribution with $T_{\mathrm{el}} > T_0$ characterizes the energy content in the electron gas.

A time-resolved measurement of the electron dynamics after fs-laser excitation with two-photon photoemission spectroscopy performed by Lisowski et al. for Ru(001) reveals for absorbed fluences of 0.4-5.6 $\mathrm{J/m^2}$ thermalization times of 110-140 fs [Lis04]. Considering the applied fluences of 50-250 $\mathrm{J/m^2}$ in the experiments reported in this thesis and the phase space argument sketched above, it is obvious that the assumption of an instantaneous thermalization is justified.

1.2.2. Electron-Phonon coupling

The coupling between electrons and phonons can be described in a model where the vibrating lattice distorts the potential which governs the movement of the electrons [Mad78]. This deformation potential describes the interaction between the valence electrons and the charged lattice ions with electron cores tightly bound to the nuclei. Using first-order perturbation theory in Born-Oppenheimer approximation, the total Hamiltonian [Gri81b]

$$\hat{H}_{\mathrm{tot}} = \hat{H}_{\mathrm{el}} + \hat{H}_{\mathrm{ion}} + \hat{H}_{\text{el-ion}} \tag{1.21}$$

includes $\hat{H}_{\mathrm{el}}$ and $\hat{H}_{\mathrm{ion}}$, which both are composed of the kinetic energy and the interaction potential of the electrons and the ions, respectively. The potential energy between electrons at position $\boldsymbol{r}_e$ and ions at $\boldsymbol{R}_i$ is considered by

$$\hat{H}_{\text{el-ion}} = \sum_{e,\,i} V_{\text{el-ion}}\left(\boldsymbol{r}_e - \boldsymbol{R}_i\right). \tag{1.22}$$

It is assumed that the deformation potential does not change when the ions are slightly displaced by $\delta\boldsymbol{R}_i$ from their equilibrium positions $\boldsymbol{R}_i^0$. Therefore, $\hat{H}_{\text{el-ion}}$ can be expressed by

$$\hat{H}_{\text{el-ion}} = \hat{H}^0_{\text{el-ion}} + \hat{H}_{\text{el-ph}}, \tag{1.23}$$

with $\hat{H}^0_{\text{el-ion}}$ describing the equilibrium positions of the ions and $\hat{H}_{\text{el-ph}}$ considering the perturbation due to phonons. The perturbation operator is then expanded to first order and quantized [Mad78, Hoh98], which then allows to interpret the electron-phonon interaction as the emission or absorption of a phonon by an electron. The energy transfer per volume and time from the electron into the phonon system is then given by the Golden Rule like expression [Mad78]

$$H\left(T_{\mathrm{el}}, T_{\mathrm{ph}}\right) = \frac{\pi}{(2\pi)^3} \sum_{\boldsymbol{q}} \hbar\omega_{\boldsymbol{q}} \int \mathrm{d}^3\boldsymbol{k}'\, W_{\boldsymbol{k}\boldsymbol{k}'} \cdot \delta\left(E_{\boldsymbol{k}} - E_{\boldsymbol{k}'} - \hbar\omega_{\boldsymbol{q}}\right) \times \left[\left(n_{\boldsymbol{q}} + 1\right) \cdot f_{\boldsymbol{k}'} \cdot \left(1 - f_{\boldsymbol{k}}\right) - n_{\boldsymbol{q}} \cdot f_{\boldsymbol{k}} \cdot \left(1 - f_{\boldsymbol{k}'}\right)\right], \tag{1.24}$$

where $f_{\boldsymbol{k}}$ and $n_{\boldsymbol{q}}$ denote the occupation numbers of the electron and phonon states, respectively. $W_{\boldsymbol{k}\boldsymbol{k}'}$ is the probability that an electron in state $|\boldsymbol{k}\rangle$ scatters into state $|\boldsymbol{k}'\rangle$ by absorption or emission of a phonon $\boldsymbol{q}$. The δ-function in Eq. (1.24) ensures the energy conservation of the transition. The first term in the squared bracket stands for the emission of a phonon, the second term denotes the absorption.

Since it is assumed that electrons and phonons are thermalized, their distribution functions are given by the Fermi-Dirac and the Bose-Einstein distribution respectively:

$$f_{\boldsymbol{k}} = \left[\exp\left(\frac{E_{\boldsymbol{k}} - E_{\mathrm{F}}}{k_B T_{\mathrm{el}}}\right) + 1\right]^{-1}, \tag{1.25}$$

$$n_{\boldsymbol{q}} = \left[\exp\left(\frac{\hbar\,\omega_{\boldsymbol{q}}}{k_B T_{\mathrm{ph}}}\right) - 1\right]^{-1}. \tag{1.26}$$

Finally, with the additional assumption that the phonon system is described by the Debye model, one obtains an energy transfer rate [Kag57, Gro95]

$$\begin{aligned} H(T_{\mathrm{el}}, T_{\mathrm{ph}}) &= f(T_{\mathrm{el}}) - f(T_{\mathrm{ph}}), \\ &\text{with} \quad f(T) = 4 g_\infty\, \theta_{\mathrm{D}} \left(\frac{T}{\theta_{\mathrm{D}}}\right)^5 \int_0^{\theta_{\mathrm{D}}/T} \frac{x^4}{\mathrm{e}^x - 1}\,\mathrm{d}x. \end{aligned} \tag{1.27}$$

Thus, the electron-phonon coupling and the energy transfer between the two subsystems of the 2-temperature model (Eq. (1.13)) can be expressed as a function of the electron and phonon temperature, respectively. The electron-phonon coupling constant g_∞ for ruthenium is denoted in Table 1.1. For a more detailed description of the above presented derivation, please see [Mad78, Hoh98, Lis05].

1.3. Adsorbate-substrate interaction: The frictional approach

Having discussed the excitation of the metal substrate in terms of an electron and phonon heat bath in the previous section, the coupling between nuclear coordinates of the adsorbate and the substrate is subject of the following considerations. The description of the coupling is based on the adiabatic frictional approach, illustrated in Section 1.1.4. Since the determined quantity in our experiments is the reaction rate, the influence of the frictional coupling strength onto Eyring's absolute rate theory is discussed subsequently, which will result in absolute desorption rates related to the coupling strength. Thus, a measure for the validity of this model approach is obtained. Finally, the key experiment for the determination of the reaction dynamics and their underlying energy transfer mechanism, namely the 2-pulse-correlation, is described.

1.3.1. Coupling between metal substrate and adsorbate

In the friction approach, adsorbate motion is assumed to occur on a single potential energy surface (PES), which is frictionally coupled to the remaining variables of the system represented by heat baths. For a conceptual approach, the PES is assumed to be a truncated harmonic oscillator. The adsorbate dynamics in the well can then be described by the harmonic oscillator master equation [Ris89]

$$\frac{\partial W_n}{\partial t} = \frac{\eta}{\mathrm{e}^{\hbar\omega/k_\mathrm{B}T_\mathrm{bath}} - 1}\left[(n+1)\,\mathrm{e}^{\hbar\omega/k_\mathrm{B}T_\mathrm{bath}}W_{n+1} + nW_{n-1} - \left(n+1+n\mathrm{e}^{\hbar\omega/k_\mathrm{B}T_\mathrm{bath}}\right)W_n\right], \tag{1.28}$$

where W_n denotes the probability of being in the nth harmonic oscillator level at time t. ω is the frequency of the adsorbate vibration along the reaction coordinate and $\hbar\omega$ therefore the oscillator level spacing. $T_\mathrm{bath}(t)$ is the transient temperature of the surrounding heat bath and η is the coupling strength. Since η has the dimension of an inverse coupling time, it represent the kinetic character of the frictional coupling.

From Eq. (1.28) a relation for the temporal evolution of the average vibrational energy U_ads of the adsorbate is derived [Bud93]:

$$\frac{\mathrm{d}}{\mathrm{d}t}U_\mathrm{ads} = \eta\left[U_\mathrm{bath} - U_\mathrm{ads}\right] \tag{1.29}$$

U_bath denotes the energy that would be in the vibration if equilibrated at T_bath:

$$U_\mathrm{bath} = \hbar\omega\left(\mathrm{e}^{\hbar\omega/k_\mathrm{B}T_\mathrm{bath}} - 1\right)^{-1}. \tag{1.30a}$$

An analog expression can be used to define an effective adsorbate temperature T_ads for any given energy content U_ads as:

$$U_\mathrm{ads} = \hbar\omega\left(\mathrm{e}^{\hbar\omega/k_\mathrm{B}T_\mathrm{ads}} - 1\right)^{-1}. \tag{1.30b}$$

Equation (1.29) describes a transient regime, where the vibrational energy of the adsorbate attempts to reach the energy which it would have in equilibrium ($T_\mathrm{ads} = T_\mathrm{bath}$), but can do so only with a finite time constant

$$\tau = \frac{1}{\eta}. \tag{1.31}$$

Since vibrational excitation of an adsorbate is the time-reversed process of vibrational relaxation, η can also be identified as a contribution to the vibrational linewidth[6] (FWHM) of the vibrational mode of frequency ω [New91].

The presented master equation approach is appropriate to describe the excitation of an intramolecular vibration where only the first few vibrational states are considered and the significant level spacing $\hbar\omega$ indicates that a quantum mechanical treatment is preferred [Mis95].

The reactants of the process investigated in the present work, however, are atomically bound to the substrate and the oscillator level spacing is close, especially compared to the high temperatures obtained after fs-laser excitation of the substrate. Therefore, a classical treatment of the adsorbate motion on the PES can be considered. The classical limit (T_{bath}, $T_{\mathrm{ads}} \gg \hbar\omega/k_{\mathrm{B}}$) of Eq. (1.29) is given by [Mis95]

$$\frac{\mathrm{d}}{\mathrm{d}t}T_{\mathrm{ads}} = -\eta\left[T_{\mathrm{ads}} - T_{\mathrm{bath}}\right], \tag{1.32}$$

where the oscillator energies U_{ads} and U_{bath} are replaced by their classical limit, namely the corresponding temperatures themselves.

The excitation of a metal substrate with laser pulses shorter than the electron-phonon equilibration time leads to huge temperature differences between the electron and phonon heat bath as shown in Section 1.2. Therefore, the adsorbate-substrate coupling must consider the two heat baths independently, which extends Eq. (1.32) to

$$\frac{\mathrm{d}}{\mathrm{d}t}T_{\mathrm{ads}} = \eta_{\mathrm{el}}\left[T_{\mathrm{el}} - T_{\mathrm{ads}}\right] + \eta_{\mathrm{ph}}\left[T_{\mathrm{ph}} - T_{\mathrm{ads}}\right], \tag{1.33}$$

where T_{el} and T_{ph} denote the electron and phonon temperature and the corresponding friction coefficients η_{el} and η_{ph}, respectively. Purely electron or purely phonon mediated processes can be considered as special cases of Eq. (1.33) with either vanishing η_{ph} or η_{el}, respectively.

1.3.2. Desorption rates

Thermally activated desorption rates R are usually given by Arrhenius-like expressions having the form

$$R = \nu_0 \exp\left(-\frac{E_{\mathrm{a}}}{k_{\mathrm{B}}T}\right), \tag{1.34}$$

where E_{a} is the height of the saddle point which has to be surmounted by the reaction partners, T is the temperature and ν_0 the so-called "attempt" frequency. The value for E_{a} is a "static property" which is usually obtained from a quantum-mechanical theory of the ground state (see Section 1.1.3). The basic problem of kinetics then concerns the value of ν_0.

The simplest approach assumes ν_0 to be equal to the frequency of vibration of the adsorbed atoms perpendicular to the surface. While this treatment seems to match a considerable number of cases for which ν_0 is between 10^{12} and $10^{13}\,\mathrm{s}^{-1}$ for first order desorption, this is a coincidence, as will be obvious from the following.

[6] In addition to the relaxation of the vibration, dephasing of an initially coherent excitation can contribute to the overall linewidth as well.

The microscopic interpretation of ν_0 uses the transition state theory developed independently by Eyring [Eyr35, Gla41] as well as Evans and Polanyi [Eva35]. (A brief derivation for a first-order process is given, since the general expression of ν_0 is not required for the further discussion, as will be seen below.) In Eyring's approach, one assumes the existence of a state of the system, called the activated complex, which corresponds to the critical configuration for reaction. This transition state corresponds to the point of no return in the movement of the system towards reaction in configuration space. For an activated reaction, it corresponds to the saddle point on the multi-dimensional potential energy surface. The concentration of the activated complex, which is by E_a higher in energy than the minimum of the PES, is given by [Gla41]

$$\sigma^\ddagger = \sigma_\mathrm{ads} \frac{f^\ddagger}{f_\mathrm{ads}} \exp\left(-\frac{E_\mathrm{a}}{k_\mathrm{B}T}\right), \tag{1.35}$$

where $\sigma^\ddagger$ and σ_ads are the surface concentrations of the transition state and the adsorbate, respectively. The f's are the corresponding complete partition functions. The activated complex can be thought of as having one loose vibrational mode ω that corresponds to the motion leading to desorption. This is expressed as $k_\mathrm{B}T/\hbar\omega$ and, when factored out of $f^\ddagger$ to give $f_\ddagger$, one obtains

$$\sigma^\ddagger = \sigma_\mathrm{ads} \frac{k_\mathrm{B}T}{\hbar\omega} \frac{f_\ddagger}{f_\mathrm{ads}} \exp\left(-\frac{E_\mathrm{a}}{k_\mathrm{B}T}\right), \tag{1.36}$$

which rearranges to

$$R = \omega\sigma^\ddagger = \sigma_\mathrm{ads}\kappa \frac{k_\mathrm{B}T}{\hbar} \frac{f_\ddagger}{f_\mathrm{ads}} \exp\left(-\frac{E_\mathrm{a}}{k_\mathrm{B}T}\right). \tag{1.37}$$

Since $\omega\sigma^\ddagger$ denotes the concentration of the activated complex multiplied by the frequency with which it leaves the transition state[7], it corresponds to the reaction rate. Note the transmission factor κ introduced in Eq. (1.37), which takes into account a certain probability of reflection at the seam of the transition state. Comparison of Eq. (1.34) and Eq. (1.37) reveals, the the pre-exponential factor for a first-order desorption process is absolutely given by

$$\nu_0 = \sigma_\mathrm{ads}\kappa \frac{k_\mathrm{B}T}{\hbar} \frac{f_\ddagger}{f_\mathrm{ads}}. \tag{1.38}$$

The meaning of "normal" ν_0 values becomes obvious from this equation. Since $k_\mathrm{B}T/\hbar \sim 1\cdot10^{12}$ to $10^{13}\,\mathrm{s}^{-1}$ for the range of 100 to 1000 K, ν_0 will be found in the same order of magnitude, if $\kappa \approx 1$ and $f_\ddagger/f_\mathrm{ads} \approx 1$.

The crucial assumption in the transition state theory (TST) of Eyring is that the transition state is in thermodynamic equilibrium with the reactants apart from the degree of freedom corresponding to the reaction coordinate. This assumption is avoided in the "diffusion model" of chemical kinetics of Kramers [Kra40] who used a classical Fokker-Planck equation for the movement of the representative point in phase-space for an analysis more general than that of Eyring. The important feature of this model is that it takes into account the coupling between the reactants and the heat bath of the solid. This coupling is represented by a friction coefficient which is exactly defined as η in the previous section. Kramers' work was applied to surface reactions by Suhl and coworkers [d'A73]. Based on this, Brenig and Schönhammer [Bre76] obtained an interpolation formula for the pre-exponential factor ν as a function of the coupling strength η which is depicted in Fig. 1.10.

[7] This implies that the transition state is traversed on the timescale of molecular vibrations, i.e. several femtoseconds.

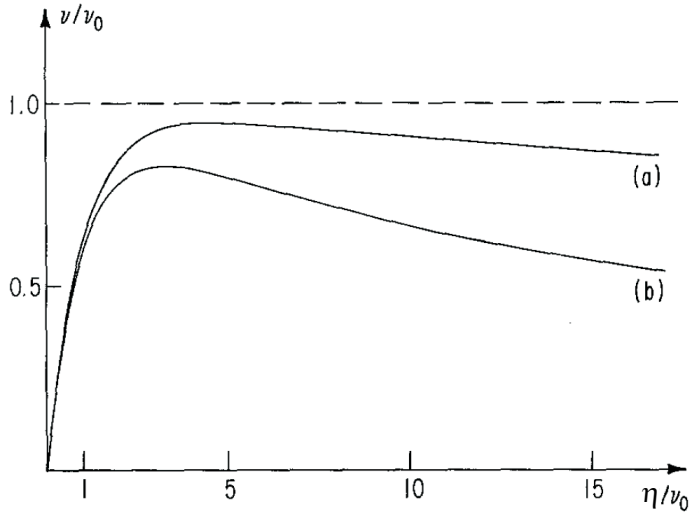

Figure 1.10.: Plot of the attempt frequency ν in terms of Eyring's absolute-rate prefactor ν_0. ν is depicted as a function of the coupling strength η for two typical values of the temperature: (a) $T = 1 \cdot 10^{-2} E_\mathrm{a}/k_\mathrm{B}$ and (b) $T = 5 \cdot 10^{-2} E_\mathrm{a}/k_\mathrm{B}$. The dotted line represents Eyring's absolute rate theory. (Taken from [Bre76])

As can be seen, for intermediate η values, the Eyring result is retained and $\nu \approx \nu_0$. For very high as well as very low η values compared to the characterictic frequency ν_0, the pre-exponentials ν become much smaller than in Eyring's case. The physical meaning is that for low η the coupling becomes so small that the rate-limiting step becomes the energy transfer. If η is large, even near the point of no return, i.e. the transition state, the motion along the reaction coordinate is hindered due to frictional damping, and low prefactors result, too. These two borderline cases are named low and high friction limit, respectively.

This behavior can also be understood in terms of molecular dynamics, where the adsorbate-substrate coupling is considered in terms of fluctuating and frictional forces both being proportional to a friction coefficient (see Appendix A). The fluctuating force governs the energy transfer into the molecular coordinates, whereas the frictional term describes the energy loss to the substrate. Thus, the low and high friction limit in Fig. 1.10 correspond to regimes where one of the two terms dominates the other.

Summarizing, one has to state that Eq. (1.34) must be extended to

$$R = \nu(\eta) \exp\left(-\frac{E_\mathrm{a}}{k_\mathrm{B}T}\right), \tag{1.39}$$

whereby the pre-exponential factor for the three different regions of frictional coupling strength is [d'A75]

$$\nu(\eta) \sim \eta/T \quad \text{for} \quad \eta < \nu_0 \cdot k_\mathrm{B}T/E_\mathrm{a} \quad \text{(low friction limit)}, \tag{1.40a}$$
$$\nu(\eta) \sim \nu_0 \quad \text{for} \quad \eta \approx \nu_0 \tag{1.40b}$$
$$\nu(\eta) \sim \nu_0/\eta \quad \text{for} \quad \eta > \nu_0 \quad \text{(high friction limit)}. \tag{1.40c}$$

For a further quantitative discussion concerning absolute reaction rates, we restrict ourselves to the low friction limit, wherefore an exact $\nu(\eta)$ can be given for the case of an parabolic potential energy surface, which is also applied for the quantitative description of the

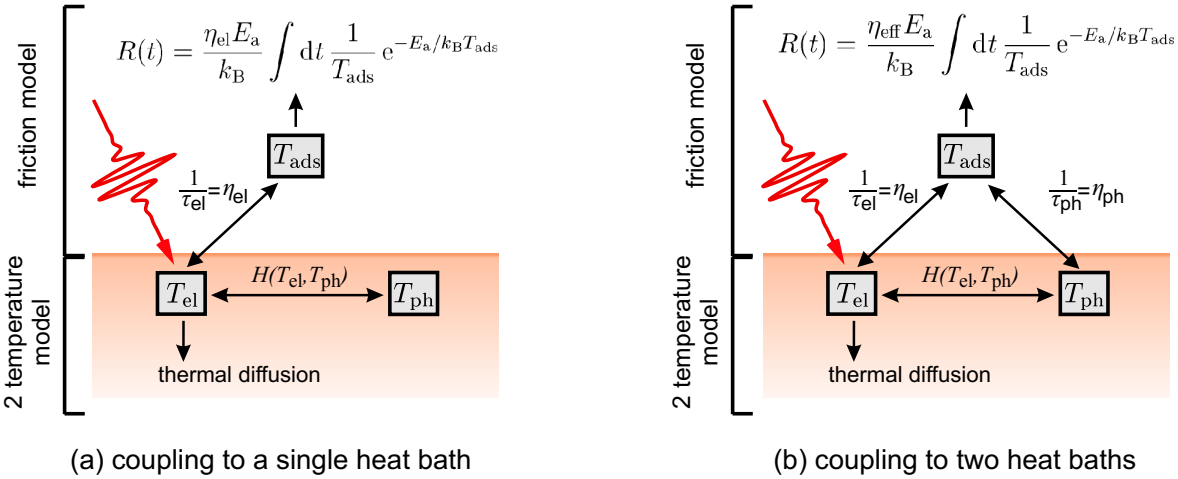

Figure 1.11.: Illustration of the adsorbate-substrate coupling in the framework of a frictional approach. (a) The adsorbate system is coupled to a single heat bath. Therefore, the modeling of the transient adsorbate temperature T_{ads} and the *absolute* reaction rate $R(t)$ is feasible with only two parameters which are the coupling strength η_{el} and the activation energy E_a for the depicted case of pure electronic coupling. (b) Coupling to two both substrate heat baths increases the parameter set for modeling to E_a, η_{el}, η_{ph} and η_{eff}. The transient electron and phonon temperatures T_{el} and T_{ph} are obtained from the 2TM (see Section 1.2).

adsorbate-substrate coupling of Section 1.3.1:

$$\nu(\eta) = \eta \cdot E_a / k_B T \qquad \text{for} \qquad \eta < \nu_0 \cdot k_B T / E_a. \tag{1.41}$$

Equation (1.41) is also valid for transient temperatures $T = T(t)$ as shown by Newns et al. [New91]. Thus, one can denote a transient reaction rate in Kramers low friction limit for an truncated harmonic oscillator and time-dependent adsorbate temperatures $T_{ads}(t)$ via

$$R(t) = \frac{\eta_{eff} E_a}{k_B} \int dt \frac{1}{T_{ads}(t)} e^{-E_a/k_B T_{ads}(t)}. \tag{1.42}$$

Equation (1.42) is used to model the experimental data in Chapter 3 and Chapter 4.

If the low friction limit is not the correct representation for the system under investigation, the reaction rate $R(t)$ can be obtained by Eq. (1.39) with either a reasonable guess for ν or an experimentally determined value. The desorption yield Y which is the measured quantity in the experiment, is then obtained as the time integral of Eq. (1.42) or Eq. (1.39) as

$$Y = \int dt\, R(t). \tag{1.43}$$

As a final remark, the impact of the presented frictional approach of adsorbate-substrate coupling and desorption is discussed: In the low friction limit and for a classical one-dimensional truncated harmonic oscillator, which is coupled to a single heat bath, the *absolute* surface reaction rate is only characterized by frictional coupling strength η and the activation energy E_a. This scenario is depicted in Fig. 1.11(a) for the special case of pure electronic coupling, i.e. $\eta_{ph} = 0$. For a purely phonon mediated reaction, the analog consideration applies as well.

In the case of a reaction where the energy transfer into the adsorbate is due to coupling to electrons and phonons, as depicted in Fig. 1.11(b), the parameter set for modeling increases

to E_a, η_{el}, η_{ph} and η_{eff}. The latter is introduced according to Mathiessen's rule in solid state physics which states that the inverse effective relaxation time of a system with different relaxation mechanisms is given by the sum of the individual inverse relaxation times [Ash01]. Thus, one obtains

$$\frac{1}{\tau_{eff}} = \frac{1}{\tau_{el}} + \frac{1}{\tau_{ph}} \quad \Leftrightarrow \quad \eta_{eff} = \eta_{el} + \eta_{el}, \tag{1.44}$$

which is used to model absolute desorption rates concerning the phonon- and electron mediated associative CO desorption in Chapter 4.

1.3.3. Isotope effect

The classical treatment of the adsorbate motion in the potential well applied in Section 1.3.1 for the electronic adsorbate-substrate coupling allows to think of η as a friction coefficient correlated to frictional forces [New91]. Thus, it can be interpreted as a friction coefficient γ normalized to the adsorbate mass m via

$$\eta_{el} = \frac{\gamma_{el}}{m}, \tag{1.45}$$

fulfilling a classical friction force representation: $F_{el} = -\gamma_{el} v$ [New91, Bra95]. As obvious from Eq. (1.33) and Eq. (1.42), an isotope effect concerning coupling times and desorption yields should be observed, with faster coupling and higher yields for the lighter isotope. The magnitude of an isotope effect depends on the difference in η for the different masses in relation to the steepness of the corresponding temperature slope. Thus, there is only a small effect for phonon-driven processes.

1.3.4. Two-pulse-correlation scheme

As mentioned before, the measurement of a 2-pulse correlation (2PC) may offer the possibility to distinguish experimentally electron- and phonon mediated energy transfer mechanisms which both might induce a reaction [Bud91, Mis92].

In such an experimental scheme, the desorption yield of the reaction is measured as a function of the delay between two almost equally intense laser pulses, as shown in Fig. 1.12. Due to the typical non-linear dependence of the yield on the absorbed laser fluence [Fri06], a correlation function is obtained whose width depends critically on the excitation mechanism. A narrow full width half maximum (FWHM) of only a few picoseconds is a clear indication for an electron driven process, since only for pulse separations shorter than the electron-phonon equilibration time the electron temperature is greatly enhanced due the combined effect of both excitation pulses. In contrast, phonon mediated processes proceed on a much slower timescale of tens of picoseconds because of the significantly longer energy storage time within the lattice compared to the electronic system. This is illustrated in Fig. 1.12.

It has to be noted that one has to be cautious of relating 2PC widths of several 10 ps only to a phonon-driven process. A FWHM of this order of magnitude clearly rules out any ultrafast purely electron mediated reaction mechanism with coupling times shorter than the electron-phonon coupling of the Ru(001) substrate. "Slow" electron mediated reaction mechanisms with coupling times larger than the electron-phonon equilibration time or a combination of

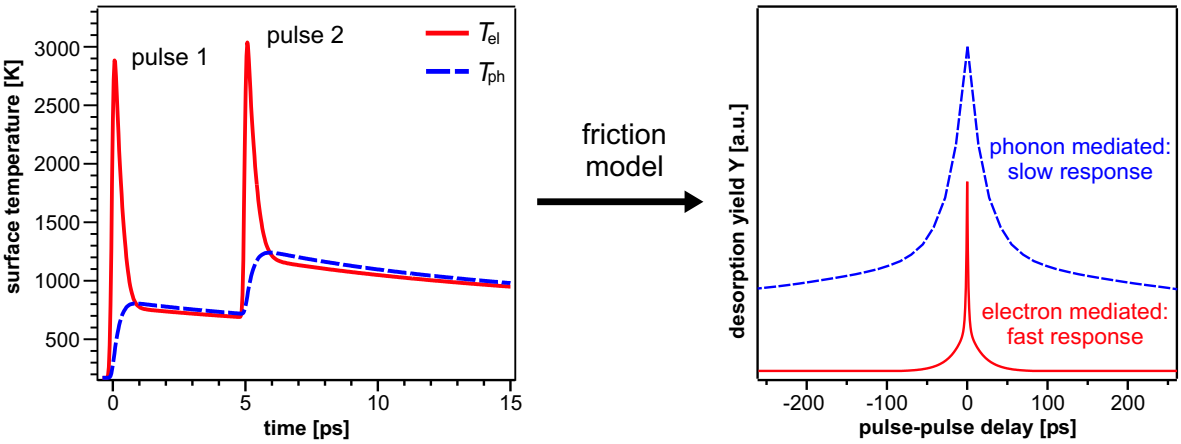

Figure 1.12.: Principle of a 2PC. On the left, electron and phonon temperatures T_{el} and T_{ph} obtained from the 2TM are plotted for two exciting laser pulses which are separated by 5 ps. The fast equilibration time exemplified for Ru(001) between T_{el} and T_{ph} is apparent. A measurement of the reaction yield as a function of the pulse-pulse delay gives a correlation function as depicted on the right. An purely electron mediated reaction is identified by a narrow 2PC width, since the second laser pulse only benefits significantly from the first one before T_{el} equilibrated to the lattice. On the other hand, phonon mediated reactions show typically a FWHM of several 10 ps.

phonon- and electron-coupling can not be resolved within a 2PC scheme. Therefore, the experimental outcome of a 2PC measurement showing a non-ultrafast correlation time has to be discussed very carefully. -phonon equilibration time or a combination of phonon- and electron-coupling can not be resolved within a 2PC scheme. Therefore, the experimental outcome of a 2PC measurement showing a non-ultrafast correlation time has to be discussed very carefully. carefully.